Microtubule dynamics. II. Kinetics of self-assembly

Henrik Flyvbjerg[1,2,3,] * and Elmar Jobs[1]
[1]*Höchstleistungsrechenzentrum (HLRZ), Forschungszentrum Jülich, D-52425 Jülich, Germany*
[2]*Department of Optics and Fluid Dynamics, Risø National Laboratory, DK-4000 Roskilde, Denmark*
[3]*Department of Physics, Princeton University, Princeton, New Jersey 08544-0708*
(Received 1 July 1997)

Inverse scattering theory describes the conditions necessary and sufficient to determine an unknown potential from known scattering data. No similar theory exists for when and how one may deduce the kinetics of an unknown chemical reaction from quantitative information about *its* final state and its dependence on initial conditions—except it is known to be impossible for equilibrium reactions. This article presents a case study of a far-from-equilibrium reaction: it presents a systematic phenomenological analysis of experimental time series for the amount of final product, a biopolymer, formed from various initial concentrations of monomers. Distinct mathematical properties of the kinetics of the unknown reaction pathway are found. These properties are shown to restrict the kinetics to a single model that generalizes Oosawa's classical nucleation-polymerization model. The methods used here to analyze the self-assembly of microtubules from tubulin are general, and many other reactions and processes may be studied as inverse problems with these methods when enough experimental data are available. [S1063-651X(97)08011-2]

PACS number(s): 87.10.+e, 82.35.+t, 87.22.Bt, 02.30Hq

I. INTRODUCTION

Scientific theories are usually not unambiguous consequences of experimental findings. The present paper describes a theory which nearly is. It is a kinetic theory, derived from experimental data for a nonequilibrium reaction. The amount of final reaction product, a polymer, is monitored in time for several traverses of the reaction pathway, traverses differing only with respect to the initial concentrations of monomers. A mathematical analysis of the resulting experimental time series leads directly to a kinetic model for the reaction pathway.

A. Inverse problem

What is solved here is a so-called *inverse problem*, i.e., an unknown cause is determined from its known effects. In physics, a classical example of an inverse problem is provided by *inverse scattering theory:* Particles are scattered off each other with various energies, and from the scattering data one tries to deduce the interaction potential between the particles. This problem is well studied, and the mathematical requirements for existence and uniqueness of a solution are understood [1,2].

In chemistry or biochemistry one can formulate an analogous inverse problem: what is the information necessary and sufficient to determine a reaction mechanism from the reaction's products? It is well known that one cannot find a unique mechanism from a kinetic analysis of a *steady-state* situation [3]. Nonequilibrium situations reveal more information, we shall see.

B. Biological self-assembly

The process studied here is an example of biological self-assembly, the spontaneous assembly of *microtubules.* Microtubules are extremely rigid protein polymers which provide rigidity where it is needed in eukaryotic cells. Self-assembly has been described for subcellular structures ranging from the simple actin polymer filaments of, e.g., muscle fibers to the highly complex *T*-even bacteriophages [4]. Models capable of quantitative reproduction of experimental data exist for the polymerization of actin [5–11] and deoxy sickle hemoglobin [12–14].

The shortage of reliable quantitative models is not due to lack of experimental data. Nor is it due to lack of interest in understanding these processes. The clinical implications for the treatment of sickle-cell anemia following from the kinetic model developed in [12–14] underscore this point dramatically. What seems to be missing is a systematic approach to the inverse problem: The self-assembly of actin polymers is sufficiently simple that the correct model could be guessed, essentially, it being the simplest possible nucleation-elongation model one can write down. Similarly, the double nucleation model for deoxy sickle hemoglobin was essentially guessed from clever experiments, and was not pushed to describe more than the initial stage of assembly.

Both actin and hemoglobin form fairly simple linear polymers, making this approach to modeling possible. More complex systems require a more systematic approach. Microtubules are polymers with a helical lattice structure, like flagella and tobacco mosaic virus, and their complexity ranks a step above that of actin and deoxy sickle hemoglobin, but below, e.g., the icosahedral capsids of spherical viruses [15].

In the present article we analyze the rich data available for the nucleation and polymerization of microtubules *in vitro* from solutions of purified tubulin. Under appropriate conditions, tubulin spontaneously assembles to form the cylindri-

*Present and permanent address: Risø National Laboratory, DK-4000 Roskilde, Denmark. Electronic address: Henrik.Flyvbjerg@Risoe.dk

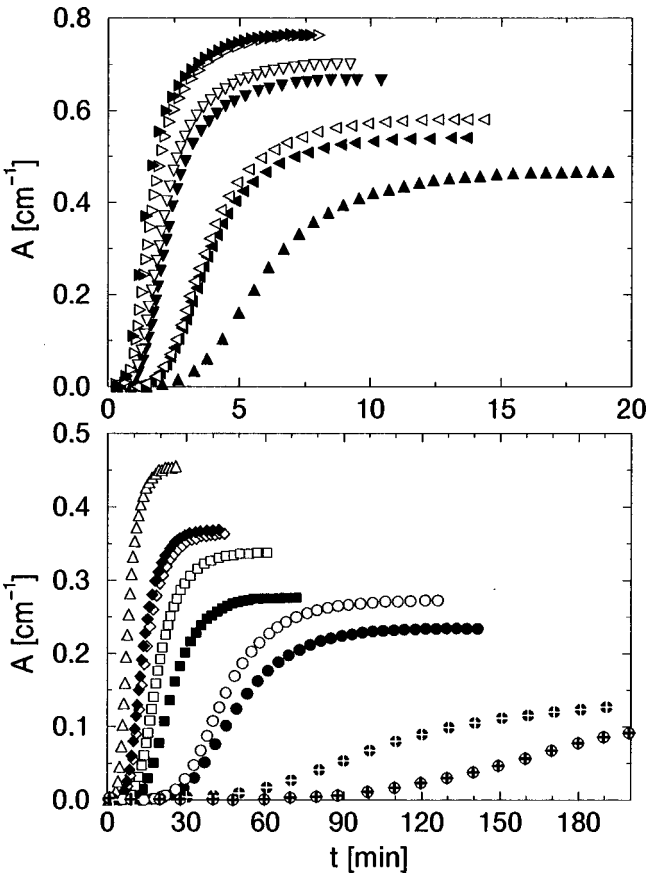

FIG. 1. Turbidity versus time of tubulin solutions in which a temperature jump from 0 °C to 37 °C at time 0 has induced microtubules to self-assemble. Open symbols: Time series obtained from eight different initial concentrations of tubulin ([17], Fig. 5), referred to as *data set A* in the present paper. Filled symbols: Time series obtained from eight independent assembly runs with eight similar initial concentrations of tubulin ([17], Fig. 9); referred to as *data set B* in the present paper.

cal five-step helical ''crystal lattice'' constituting a microtubule, see [16] Fig. 1. During the assembly reactions discussed below, α and β tubulin monomers are permanently bound together in pairs, tubulin hetero-dimers, which therefore are *effective monomers* of the reactions studied. So whenever we use the word ''monomer'' in the following, we are referring to these effective monomers.

C. Turbidity time series

The data analyzed here are shown in Fig. 1: The plotting symbols are experimental time series for the *turbidity A* of 16 different solutions of tubulin in which microtubules grow in the presence of glycerol [17]. The turbidity is a simple and precise physical measure of the amount of tubulin that has polymerized at any given time during assembly; see below. These time series define our inverse problem: we assume that they all resulted from the same assembly pathway, initiated with different initial concentrations, and then try to find that pathway from the time series. As in [17], we will distinguish between the eight time series measured in one set of assembly runs and shown with filled symbols, and the other eight series measured in another, independent set of assembly runs and shown with open symbols. We refer to them as data sets *A* and *B*, respectively.

The model we find here generalizes the classical model by Oosawa and co-workers [5–7]. It is analytically soluble up to one integral despite its highly nonlinear nature. More important, though a specific reaction is analyzed here, the methods used are general, and may be applied to a wide range of reactions, provided sufficient experimental data are available.

D. The logical steps

The logical steps leading to the assembly kinetics may be summarized as follows. First, we observed that the time series seem to *scale*. We therefore analyzed them for this property, and found that they display so-called *phenomenological scaling* to a good approximation.

If this scaling property were exact, the individual time series would be fully characterized by one characteristic turbidity scale and one characteristic time scale, while its overall behavior is common to all the time series, and described by a single function. This simple phenomenology is typically displayed by processes which are dominated by or consist of a single mechanism. It vastly simplifies the task of modeling, because all series are described by the same unknown function, rather than each series by its own. For this reason, we demanded that our unknown theory should scale, knowing that it would only be an approximate theory then, but a good approximation.

Second, we considered the dependence of the characteristic time on the characteristic turbidity. Both were read off the experimental time series, so their relationship could be found without knowing the assembly kinetics. We found a remarkably simple and robust relationship, namely, that the characteristic time is inversely proportional to the third power of the final turbidity.

Third, we interpreted these results as indicating simplicity of the assembly process, hence assumed a single pathway of assembly would be adequate to describe the experimental data. We wrote down a generic model for this and demanded that its solutions scale as just described. We found that these requirements *uniquely determine* the model up to the number of assembly steps in it, and the values of the rate constants for these steps.

Fourth, we realized that the number of assembly steps is revealed in the initial growth of the time series, and analyzed this growth. We found that the series grow with time to the sixth power. This result means that a stable nucleus for polymerization is created in *five* steps and is made from 18 tubulin hetero dimers. Thus the kinetic model was uniquely determined up to five rate constants.

Fifth, we solved the kinetic model exactly up to a single integral. The model is described by six coupled nonlinear first-order differential equations in time, but because of their scaling properties, these equations can, nevertheless, be solved.

Sixth, we fitted the solution of the kinetic model to the experimental time series, using the five rate constants as fitting parameters. Four of these rate constants set the rates for similar processes, and turned out to have identical values when fitted to the data. So we might as well *assume* those four rate constants to be equal, and work with a two-parameter theory. That theory is our final model, and is the

one shown fitted to the experimental data in Figs. 9–11.

A brief version of the analysis presented here was given in [18]. The present paper is the second of three that all apply the modeling tools of theoretical physics to different aspects of the complex dynamics of microtubules. The first paper [16] modeled the cause of so-called *dynamic instability* [19,20], a phenomenon observed in microtubules that have not been stabilized like those discussed here. Specifically, the stochastic dynamics of the so-called *cap* was modeled, and found to provide a common explanation of different experiments. The third paper will more thoroughly discuss a realistic model of so-called *microtubule oscillations* which was briefly presented in [21] and builds on the modeling presented here and in the first paper of the triology.

II. PHENOMENOLOGICAL DATA ANALYSIS

A. The scaling ansatz

The experimental time series shown in Fig. 1 all have similar sigmoid shapes. We therefore ask whether they differ only through different overall time and turbidity scales. If this is the case, they are said to *scale*, meaning all 16 time series can be described by a *single* function f as

$$A(t;A_\infty)=A_\infty f(t/t_0(A_\infty)), \tag{1}$$

a property which obviously would reduce the task of modeling significantly. Here f is a dimensionless function of a dimensionless argument, and interpolates between 0 and 1. In Eq. (1) we distinguish the 16 time series and corresponding characteristic times t_0 by the asymptotic value A_∞ of the individual time series. These asymptotic values are easily determined with precision from the series, as we shall see.

The relationship (1) is more easily determined by plotting A against t with double-log axis, since Eq. (1) implies that

$$\log_{10}A=\log_{10}A_\infty+g(\log_{10}t-\log_{10}t_0), \tag{2}$$

where $g(x)=\log_{10}[f(\exp x)]$. Equation (2) shows that if scaling is satisfied, different time series fall on curves which are identical, apart from being translated vertically and horizontally relative to each other by amounts given by $\log_{10}A_\infty$ and $\log_{10}t_0$, respectively.

The experimental time series in Fig. 1 are replotted with double-log axis in Fig. 2. We see, indeed, that the series seem to be translates of each other with few exceptions which we shall return to. In order to test the validity of this similarity, we need to find t_0 and A_∞ for each individual time series, translate the plots of the series by these amounts, and inspect the degree of collapse of the resulting plots.

B. Determining A_∞

The asymptotic turbidity A_∞ can be obtained with better precision than any other number we shall discuss, because A_∞ is approached exponentially fast in time, i.e., in a simple and distinct manner that allows us to extrapolate from the data at late, but finite, times to a value for A_∞ which truly corresponds to time infinity. At this point in our line of deduction, it is a purely phenomenological observation that this approach is exponential. The observation is made for a given time series, and its value for A_∞ is determined with precision,

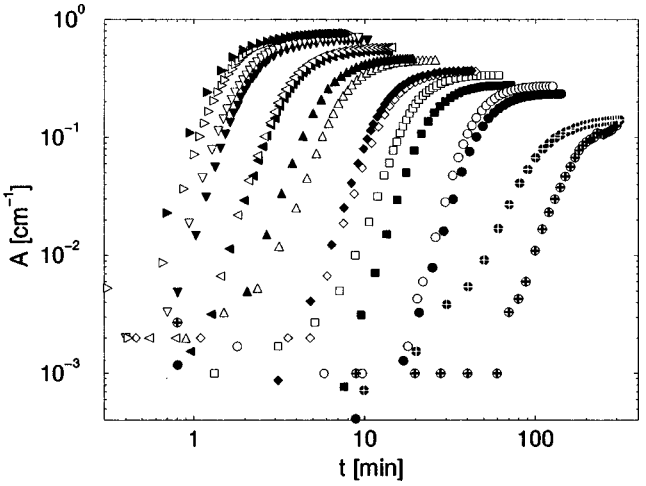

FIG. 2. Same data as in Fig. 1, plotted as $A(t)$ against time t using double-log axis.

by finding the value for A_∞ which gives the best straight-line fit to $\log_{10}[A_\infty-A(t)]$ plotted against t at late times. While this procedure may be ambiguous in general, it is not in the present case, because the exponential approach is very distinct in the data. Figure 3 shows that approximately the last third of the data points in each time series displays this exponential approach to its asymptotic value.

C. Why A_∞ is approached exponentially fast

From a theoretical point of view, an obvious interpretation of this exponential approach offers itself. The amount of polymer present, hence the turbidity A, grows at a rate which is proportional to the number of microtubules, $\nu(t)$, and to the remaining amount of tubulin, $c(t)$,

$$\frac{dA(t)}{dt}\propto\nu(t)c(t). \tag{3}$$

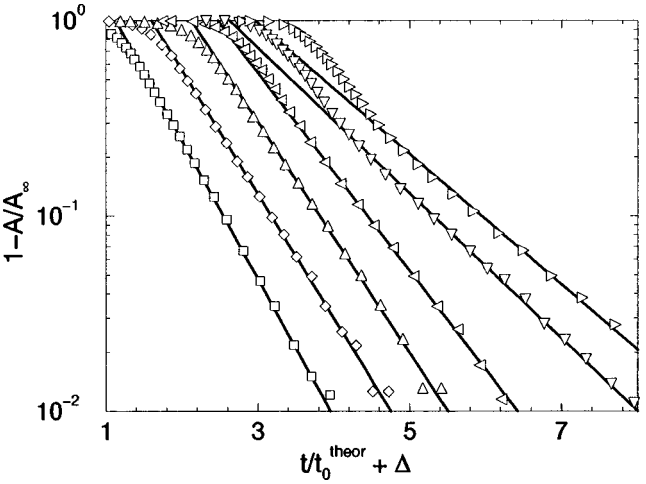

FIG. 3. Demonstration that a turbidity time series approaches its asymptotic value, A_∞, exponentially fast in time. $A_\infty-A(t)$ plotted against t. $A(t)$ is an experimental time series, while A_∞ is a value chosen for each series so as to make $A_\infty-A(t)$ fall on a straight line at late times in this plot. t is given here in units of a characteristic time, t_0^{theor}, which is introduced below, and here only serves to make it possible to show several time series in one plot. The offset Δ serves the same purpose.

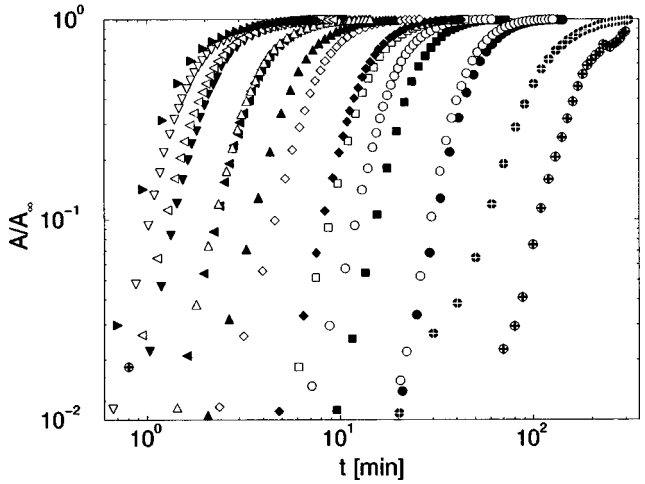

FIG. 4. Same data as in Fig. 1, plotted as $A(t)/A_\infty$ against time t using double-log axis.

The microtubules in these experiments are stabilized with glycerol and cannot depolymerize again, once they have formed, so we may assume that all the tubulin initially present in solution eventually ends up being polymerized. Then

$$c(t) \propto A_\infty - A(t), \tag{4}$$

hence

$$\frac{dc(t)}{dt} \propto -\nu(t)c(t). \tag{5}$$

If, as expected, nucleation of microtubules is a cooperative process involving several tubulin molecules, then nucleation of new microtubules will terminate faster than the polymerization of already existing microtubules, because the latter is proportional to $c(t)$ while nucleation depends on a higher power of $c(t)$. Consequently, $\nu(t)$ will reach its asymptotic value ν_∞, faster than $c(t)$ reaches *its* asymptotic value, 0, and at late times we have

$$\frac{dc(t)}{dt} \propto -\nu_\infty c(t), \tag{6}$$

which shows that $c(t)$, hence $A_\infty - A(t)$, vanishes exponentially fast in time, as we found for the experimental time series.

If we accept this interpretation of the late third of each time series, we must obviously extract information about the nucleation process from the initial two-thirds of the series. Not even the final number of microtubules, ν_∞, can be determined from the late part of the experimental time series. This is because the turbidity measures only the total amount of polymer present, i.e., the summed length of microtubules present, and cannot distinguish many short microtubules from fewer, longer microtubules.

D. Determining t_0

Having determined A_∞ for each time series, we replot the series as $A(t)/A_\infty$ vs t with double-log axis. This was done in Fig. 4, and the series do seem to be identical up to a translation along the log$t$ axis, except for the two slowest assembling series, marked with crosses inside circles.

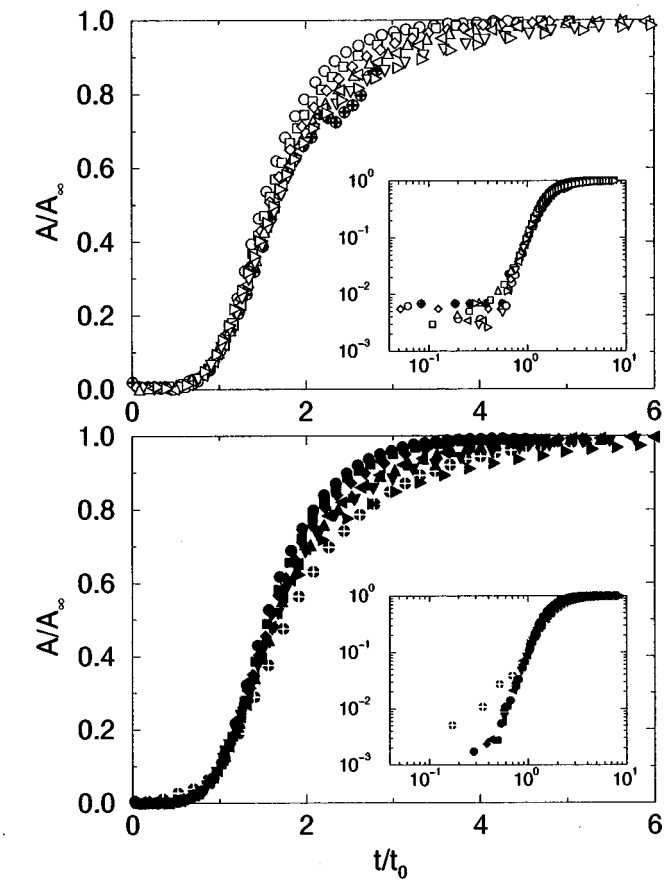

FIG. 5. Experimental data from Fig. 1, replotted here with the same plotting symbols, but as A/A_∞ against t/t_0, demonstrating data collapse. Open symbols: data set A. Filled symbols: data set B. Insets: same plotted with double-log axis.

To test for this last property, we read the so-called *tenth time*, t_0, off Fig. 4 for each time series. The *tenth time* is the time when a series has reached one-tenth of its final value. The choice of one-tenth is conventional [17], and convenient for our purpose, since we can easily obtain the tenth time with precision from Fig. 4. We then replotted the series as A/A_∞ against t/t_0 in Fig. 5. Other definitions, e.g., half time, can be used and lead to similar results.

E. Data collapse

Figure 5 shows that the relationship in Eq. (1) does, indeed, hold to a high degree for almost all of the time series. Only the two time series plotted as crosses within circles appear anomalous. They describe the two *slowest* assembly experiments, starting with the *lowest* concentrations of tubulin, and lasting for over two hours. *Aging* of tubulin is well known to occur over such long times at 37 °C, and may be responsible for their anomalous forms. We exclude these series from the analysis on this ground. They define one side of the experimental window for microtubule assembly.

Any sensibly chosen curve representing the remaining time series would differ at most 10% from the worst case at the worst time. So even before we know the theory that we

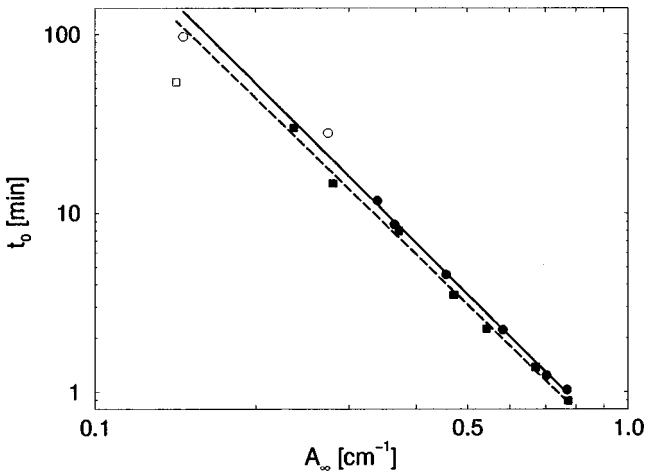

FIG. 6. Double-log plot of $t_0(A_\infty)$ vs A_∞. Circular symbols show results for data set *A*. The full straight line is a fit to the six *filled* round symbols which most distinctly fall on a straight line. Its slope is -2.97 ± 0.05. The two time series corresponding to the two *open* round symbols appear anomalous, maybe because they describe the slowest assembly processes in data set *A*, and tubulin at 37 °C denaturates after a while. But their inclusion in the fit obviously would not change its outcome. Square symbols show results for data set *B*. The dashed straight line is a fit to the seven filled square symbols which most distinctly fall on a straight line. Its slope is -2.90 ± 0.09. The intercepts of the two straight lines with the second axis do not differ significantly, and give the constant of proportionality in Eq. (7) as 0.44 ± 0.03 min/cm^3.

are looking for, we know which precision we may achieve with it.

In the remaining time series, it is the time series corresponding to the *highest* initial concentrations and *fastest* assembly dynamics that differ from the others at late times in Fig. 5. This is so for both data sets *A* and *B*, and shows that the discrepancy is systematic. It is known from electron microscopy that at these highest concentrations, in addition to microtubules, other assembly products also form [17]. This is a good reason not to worry about the way these time series differ from the rest when they do—they are close to the other side of the experimental window for microtubule assembly. Instead, we focus on the fact that the other series coincide well.

Experimental data are always noisy on some scale, hence can never display a perfect collapse. The imperfection of the data collapse in Fig. 5 is not due to the experimental error bars that we estimate below, however. So it is a matter of taste and preference whether one accepts the collapse as such. We do, because it is a great mathematical convenience, potentially leading to a theory that is at least 90% correct. Once that scaling theory has been established, one may try to describe the last 10% difference between theory and experimental data as *scaling violations*, using a perturbative approach with the 90%-correct theory as the starting point and leading approximation.

F. The relationship between A_∞ and t_0

The values for t_0 that we read off Fig. 4 are plotted against the corresponding values for A_∞ in Fig. 6. This figure shows quite convincingly that

$$t_0 \propto A_\infty^{-3}. \tag{7}$$

This relationship is surprisingly simple. Like the scaling property, this simplicity indicates that a single pathway is responsible for the assembly reaction studied here, even though the total amount of tubulin polymerized in these reactions varies by a factor larger than 3, and their time scales by a factor larger than 30. Both the scaling property (1) and the power-law dependence (7) are of a precise mathematical form. Thus, without use of any theory, whatsoever, our phenomenological analysis of the data has revealed mathematical properties which, if demanded from a model, will narrow the search for this model significantly.

Fitting the integer power law (7) to the combined data in Fig. 6 gives the prefactor and what we shall refer to as our *theoretical* value for t_0 for a given value of A_∞, in order to distinguish it from the relationship read of the individual time series,

$$t_0^{\text{theor}}(A_\infty) = (0.41\pm0.01)\ \text{min/cm}^3 \times A_\infty^{-3}. \tag{8}$$

III. MODELS

Voter and Erickson considered three theoretical models for their experimental time series [17]: (i) The classical model by Oosawa and co-workers [5–7], which is the simplest possible theory describing nucleation followed by polymerization. It describes formation of a nucleus in a single step. Experimental results for the spontaneous self-assembly of *actin filaments*, which are relatively simple helical polymers, are fitted well by this model [11]; (ii) a double-nucleation model devised for the spontaneous polymerization of *deoxy sickle hemoglobin* [14]. This model has already formed polymer catalyze the nucleation of more polymers; and (iii) a model for two-dimensional nucleation and polymerization inspired by the geometrical form of microtubules. Neither of these models described the time series well [17].

In view of this, we formulated a *generic* class of *phenomenological* models which describe the formation of a nucleus through *any* sequence of intermediate stages, assuming only a *single* sequence, or path of assembly, is involved; see Fig. 7. In principle, several different paths of assembly may contribute simultaneously to the formation of microtubules. If this is the case, it is hardly possible to separate and determine these paths from the turbidity time series alone, because different paths typically will contribute to the turbidity with different weights at different initial tubulin concentrations. That is why we tentatively assumed that there is only one path of self-assembly (cf. [22]). We also assumed that every stage in this path is connected to the next stage by addition of monomers only. This second assumption is very reasonable because the monomer concentration greatly exceeds any other concentration while nucleation takes place. With these two assumptions, we could write down a generic set of kinetic equations describing the assembly process. According to *Occam's Razor*, this model is then correct if it works. If it does not, that is also a definite result about the complexity of the data. We found the assumption confirmed by the results it leads us to, or, more correctly, we found it justified as a very good and practical first approximation. We

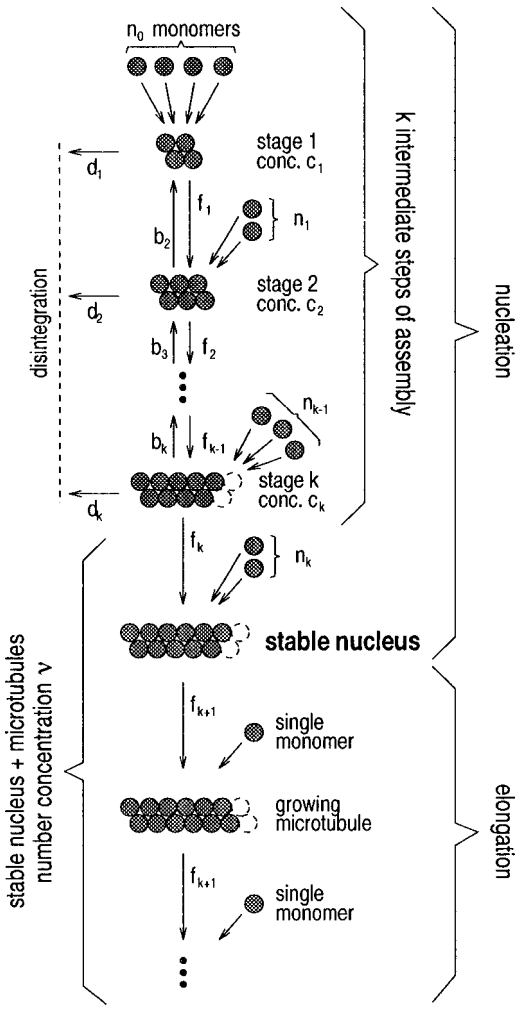

FIG. 7. Kinetics of assembly of nucleus from monomers with concentration c through several relatively stable intermediate aggregates. For $1 \leqslant i \leqslant k$, f_i is the rate constant for the assembly of the $(i+1)$th relatively stable aggregate, having concentration c_{i+1}, from the ith such aggregate, having concentration c_i, by addition of n_i monomers. b_i is the rate constant for the reverse process, and d_i the rate constant for disintegration of the ith aggregate. The $(k+1)$th aggregate is the nucleus, defined as the smallest aggregate to which further addition of monomers takes place one at a time, and at the rate with which microtubules grow. The number concentration of these nuclei *and* longer microtubules is ν, and the concentration of polymer mass accumulated in them is M.

will briefly return to the possibility of multiple pathways in Sec. XII C.

Let c denote the monomer concentration, c_i the number concentration of the ith relatively stable intermediate assembly product, n_i the number of monomers added to this product to form the $(i+1)$th intermediate assembly product, k the number of different, successive intermediate products—i.e., k is the number of intermediate assembly stages of the nucleus— and ν the number concentration of nuclei, including such on which microtubules have grown. Let M denote the amount of mass polymerized to microtubules, discounting the mass in nuclei and intermediate assembly products, since the latter do not contribute to the turbidity. With this notation, and f_i, b_i, and d_i denoting forwards, backwards, and disintegration rate constants, respectively, the kinetic equations are

$$dc_1/dt = f_0 c^{n_0} - f_1 c^{n_1} c_1 + b_2 c_2 - d_1 c_1, \tag{9}$$

$$dc_i/dt = f_{i-1} c^{n_{i-1}} c_{i-1} - f_i c^{n_i} c_i - b_i c_i + b_{i+1} c_{i+1} - d_i c_i \quad \text{for } 2 \leqslant i \leqslant k, \tag{10}$$

$$d\nu/dt = f_k c^{n_k} c_k, \tag{11}$$

$$dM/dt = f_{k+1} c \nu. \tag{12}$$

The addition of $n_i > 1$ monomers in one step at a rate proportional to c^{n_i} is the effective kinetic description that results when one is unable to time resolve n_i rapid successive additions of a single monomer, in equilibrium with the quick decay of the highly unstable intermediate aggregates formed. Since $n_i = 1$ is allowed in Eqs. (9)–(11), any degree of experimental time resolution can be captured with these equations, including perfect resolution.

$f_{k+1} c$ is the rate at which microtubules grow at tubulin concentration c. We have set the backwards rates b_i and the destruction rates d_i to zero for $i \geqslant k+1$, assuming microtubules can only grow. This is what we expect for microtubules stabilized with glycerol, as in [17]. It is what was found experimentally for microtubules stabilized with a nonhydrolyzable GTP (guanosine triphosphate) analog ([23], Fig. 3). It has also been demonstrated experimentally for nonstabilized microtubules in the growing state [24].

IV. RELATING EXPERIMENTAL AND THEORETICAL VARIABLES

When self-assembly is initiated at $t = 0$, only monomers are present. Since nuclei form with difficulty, while microtubules grow rapidly, the amount of tubulin contained in nuclei and intermediate aggregates is negligible at any time during assembly, compared to that in monomer or polymer form. If we neglect the negligible, mass conservation gives us

$$c + M = c(0), \tag{13}$$

where $c(0)$ is the monomer concentration at time $t = 0$. For comparison and later consistency check, the exact relationship is

$$c + n_0 c_1 + (n_0 + n_1) c_2 + (n_0 + n_1 + n_2) c_3 + \cdots + \left(\sum_{i=0}^{k-1} n_i \right) c_k + \left(\sum_{i=0}^{k} n_i \right) \nu + M = c(0). \tag{14}$$

We checked the consistency of the approximation (13) by using it when solving the theory derived below, and inserting the solution into the additional terms occurring in Eq. (14). As they turned out to be negligible at all times, the approximation (13) is self-consistently correct.

This is a crucial result because we cannot use the exact relationship (14). Only Eq. (13) enables us to relate the experimentally measured variable, the turbidity, to the theoretically relevant variable, the tubulin concentration, in a manner that preserves the precision with which the turbidity is known. Equation (12) shows that M will keep growing until $c = 0$, so from Eq. (13) follows that $M(\infty) = c(0)$. As ex-

plained in the next subsection, the turbidity A is proportional to the amount of polymerized tubulin M, so we have

$$A(t)/A_\infty = M(t)/M(\infty) = 1 - c(t)/c(0). \tag{15}$$

With this simple relationship we avoid corrupting the precision of the data with biochemical assays of $c(0)$ and of the relationship between turbidity and polymerized tubulin. Instead, we work with the relative variable $c(t)/c(0)$, and use Eq. (15) to relate this theoretical variable to the experimentally measured variable $A(t)$, a crucial practical point in our analysis.

A. Why $A(t) \propto M(t)$

We have considered and excluded the possibility that the initial lag in turbidity in Fig. 1 is an artifact due to short microtubules contributing less to the turbidity [25]. The turbidities in Fig. 1 were measured with 350 nm light. At this wavelength, monomers and oligomers are transparent, while microtubules longer than the wavelength— i.e., microtubules containing more than 600 monomers— contribute to the turbidity with an amount that is proportional to their length to a very good approximation ([25], Fig. A2).

Our analysis of the turbidity time series in Fig. 1 show that microtubule nucleation has dropped to less than 2% of its initial rate when microtubule polymerization has reduced the tubulin concentration to less than half of its initial value. Microtubules polymerized after that point in time contribute even less than 2% to the total turbidity. Ignoring the latter microtubules, microtubules grow to a length of 350 nm in times that are negligible relative to the characteristic times of the turbidity time series. This is seen as follows: For lack of a direct measurement of the microtubule growth rate, we interpolate results obtained in other buffers and at other temperatures [24,26–28], and estimate the rate in the buffer and at the temperature used in [17] to be approximately 1 μm/min/(μM tubulin). Consequently, in the most sensitive case, that of highest initial tubulin concentration, 19.0 μM, microtubules nucleated at half that concentration grow to 350 nm in 2 sec. This initial time interval, in which a microtubule does not contribute to the turbidity with an amount proportional to its mass, is negligible. For comparison, the origin of time is defined by the temperature ''jump'' initiating nucleation; it lasts 15 sec [17].

V. CONSEQUENCE OF SCALING LAWS

We need not solve Eqs. (9)–(15) before we look for solutions satisfying the scaling laws (1) and (7). Instead, we impose as a *demand on the equations* (9)–(15) that their solutions satisfy the scaling laws. This simplifies the equations very much, hence eases our task of solving them.

The demand is implemented by rewriting the generic equations (9)–(12) in terms of scaling variables, t/t_0, c/c_0, c_i/c_0^m, $M/M(\infty) = M/c_0$, where $t_0 \propto c_0^{-m}$. Here we have introduced the shorthand notation c_0 for $c(0)$ and a parameter m which, according to Eq. (7), has the value 3. In order to demonstrate the generality of our approach, arguments, and results, we treat m as if its value is unknown for as long as we can.

Having rewritten the kinetic equations in terms of the scaling variables, one demands that c_0 does not appear explicitly anywhere in the equations, but only implicitly, through the scaling variables. It is this demand which ensures that solutions obey the scaling laws. It also forces many terms out of the equations, because they contain explicit powers of c_0. It restricts the possible kinetics to just one set of equations:

$$dc_1/dt = f_0 c^{2m} - f_1 c^m c_1, \tag{16}$$

$$dc_i/dt = f_{i-1} c^m c_{i-1} - f_i c^m c_i \quad \text{for } 2 \leqslant i \leqslant k, \tag{17}$$

$$d\nu/dt = f_k c^m c_k, \tag{18}$$

$$dM/dt = f_{k+1} c \nu. \tag{19}$$

While coupled nonlinear differential equations in general are not analytically solvable, this particular set is to quite an extent.

VI. ANALYTICAL SOLUTION OF MODEL

The relevant initial condition for Eqs. (16)–(19) is one with only tubulin present at time $t=0$: $c = c_0$, $c_1 = c_2 = \cdots c_k = \nu = M = 0$.

Eliminating M, ν, c_k, . . . , c_2, and c_1 from these equations, we find that c satisfies the equation

$$\left(\prod_{i=1}^{k} \left[c^{-m} \frac{d}{dt} + f_i \right] \right) \left[c^{-m} \frac{d}{dt} \right]^2 c^m = -m \left(\prod_{i=0}^{k+1} f_i \right) c^m, \tag{20}$$

with initial condition

$$c(0) = c_0, \quad \frac{d^i c}{dt^i}(0) = \quad 0 \text{ for } i = 1,2,\ldots,k,k+1. \tag{21}$$

While nonlinear $(k+2)$th-order differential equations in general are not analytically solvable, this particular one is. We introduce alternative variables τ and γ,

$$\tau = \int_0^t c^m(t')\,dt', \tag{22}$$

$$\gamma(\tau) = [c(t)/c_0]^m. \tag{23}$$

These definitions were chosen to have $c^{-m} d/dt = d/d\tau$, so that the nonlinear differential equation (20) simplifies to a linear differential equation

$$\left[\frac{d}{d\tau} \right]^2 \left(\prod_{i=1}^{k} \left[\frac{d}{d\tau} + f_i \right] \right) \gamma = -m \left(\prod_{i=0}^{k+1} f_i \right) \gamma. \tag{24}$$

This equation can be solved for γ as a function of τ,

$$\gamma(\tau) = \sum_{i=0}^{k+1} \left(\prod_{\substack{j=0 \\ j \neq i}}^{k+1} \frac{z_j}{z_i - z_j} \right) \exp(z_i \tau), \tag{25}$$

where $z_i, i = 0, \ldots, k+1$, are the $k+2$ roots of the polynomial

$$z^2(z+f_1)\cdots(z+f_k)+mf_0f_1\cdots f_{k+1}, \tag{26}$$

and we have used that the initial condition translates to

$$\gamma(0)=1, \quad d^i\gamma/d\tau^i(0)=0 \quad \text{for } j=1,\ldots,k+1. \tag{27}$$

The solution for $c(t)$ is then obtained in parametric form,

$$t=c_0^{-m}\int_0^\tau d\tau'\,\gamma^{-1}(\tau'), \quad c(t)=c_0\gamma^{1/m}(\tau), \tag{28}$$

where the integral is known analytically only in the case of $k=0$, i.e., for Oosawa's model.

In all these equations, f_0 and f_{k+1} occur only through the product $\Pi_{i=0}^{k+1}f_i$, and are furthermore invariant under permutations of $f_1, f_2, \ldots, f_k$. This is so because the turbidity depends on only the total summed length of polymers formed, and not on its distribution on microtubules, nor on the concentrations of intermediate aggregates. This property then carries over to $M(t)$ and $c(t)$ by Eq. (15). Consequently, any solution to these equations will depend on f_0 and f_{k+1} only through their product, and on $f_1, f_2, \ldots, f_k$ in a manner that is invariant under permutations. Thus a fit of such a solution to experimental data using $f_0, f_1, \ldots, f_{k+1}$ as fitting parameters can never determine them all, but only $f_1, \ldots, f_k$ and the product f_0f_k. Furthermore, for any fitted set of parameters in which the f_is are not identical for $i=1,\ldots,k$, there are other parameter sets giving exactly the same fit, namely, all permutations of $(f_1, \ldots, f_k)$.

Equations (16)–(19) are just one set out of a class of similar sets of equations characterized by two parameters m and k. All these nucleation-polymerization models are analytically solvable but for one integral. The case of $k=0$, i.e., nucleation in a single step from monomer to nucleus, is Oosawa's model, and fully solvable with

$$c(t)=c_0\cosh^{-1/m}([mf_0f_1c_0^{2m}]^{1/2}t). \tag{29}$$

VII. DETERMINING THE NUMBER OF EQUATIONS

At this point in our analysis we have found more than we need, a whole class of soluble nucleation models, parametrized by the two integers m and k. We know that $m=3$, but have yet to determine k from the experimental data. This amounts to determining the number of equations in the theory (16)–(19) from the data that the theory is meant to describe. This is done by observing that all the equations (16)–(19) are first-order differential equations in time—as kinetic equations are—and that the variables they describe, $(c_i)_{i=1,\ldots,k}$, ν, and M, all vanish initially, while each one of them initially increases at a rate proportional to the value of the previous one. Consequently, $M(t)\propto t^{k+2}$ initially, and the number of equations follows from $M(t)$'s growth at early times. The following subsection details this.

A. Initial assembly kinetics: Theory

The kinetics at early times is described by solving Eqs. (16)–(19) to leading order in t. To this end we note that only c differs from zero initially, $c(0)=c_0$, while $c_1=c_2=\cdots=c_k=\nu=M=0$ initially. c_1 is initially created at a constant rate, $f_0c_0^{2m}$, so c_1 initially grows proportional to t. Since c_2 is created at a rate proportional to c_1, c_2 initially grows proportional to t^2. c_3 grows at a rate proportional to c_2, hence proportional to t^3 initially. And so on, with M growing proportional to t^{k+2} initially. Only with M's increase from zero does $c(t)$ decrease from c_0, i.e., $c(t)=c_0-O(t^{k+2})$. So to leading nonvanishing orders we have initially that

$$c_1(t)=f_0c_0^{2m}t+O(t^2), \tag{30}$$

$$c_2(t)=f_0f_1c_0^{3m}t^2/2+O(t^3), \tag{31}$$

$$\vdots$$

$$c_k(t)=\left(\prod_{i=0}^{k-1}f_i\right)c_0^{(k+1)m}t^k/k!+O(t^{k+1}), \tag{32}$$

$$\nu(t)=\left(\prod_{i=0}^{k}f_i\right)c_0^{(k+2)m}t^{k+1}/(k+1)!+O(t^{k+2}), \tag{33}$$

$$M(t)=\left(\prod_{i=0}^{k+1}f_i\right)c_0^{(k+2)m+1}t^{k+2}/(k+2)!+O(t^{k+3}). \tag{34}$$

From Eq. (34) we see that a plot of $\log_{10}[A(t)/A_\infty]=\log_{10}[M(t)/M(\infty)]$ against $\log_{10}(t/t_0)$ should start out at early times t as a straight line with slope $k+2$ independent of initial concentration c_0.

The inset in Fig. 5 shows the experimental data plotted this way. The very earliest data points shown, those having $A/A_\infty<10^{-2}$, are not measures of turbidity, but indicate the limit of the turbidimeter's sensitivity. Later points initially fall on a straight line with a slope that we now determine.

B. Initial assembly kinetics: Phenomenology

Some care is required in order to extract an asymptotic behavior from noisy data. One can choose between robust methods that willingly yield a result—which may be wrong without much warning—and more refined methods that demand more from the data to function, but also give information about a result's reliability. In [18] we used a robust noise reduction method to obtain a value for the number of equations, and found the value $k+2=4.96$. That result was seducingly close to an integer value, as it should be, but this was also the only cross-check we had on the result, and it could be the outcome of chance.

In the present paper we apply a more systematic and more demanding method, and find k falls between 3 and 4, with the value 4 being favored. We fitted

$$at^{k+2}+bt^{k+3} \tag{35}$$

to the initial part of each time series, using a, b, and k as unknown, real fitting parameters, and fitting to data points up to a cutoff time, measured in units of the characteristic time t_0 for each time series. The degree of justification with which we may use Eq. (35) to describe the *individual* time series' early behavior is indicated by the size of the equation's first term compared to its second term for t equal to the cutoff time. With a k value found in this manner for each time

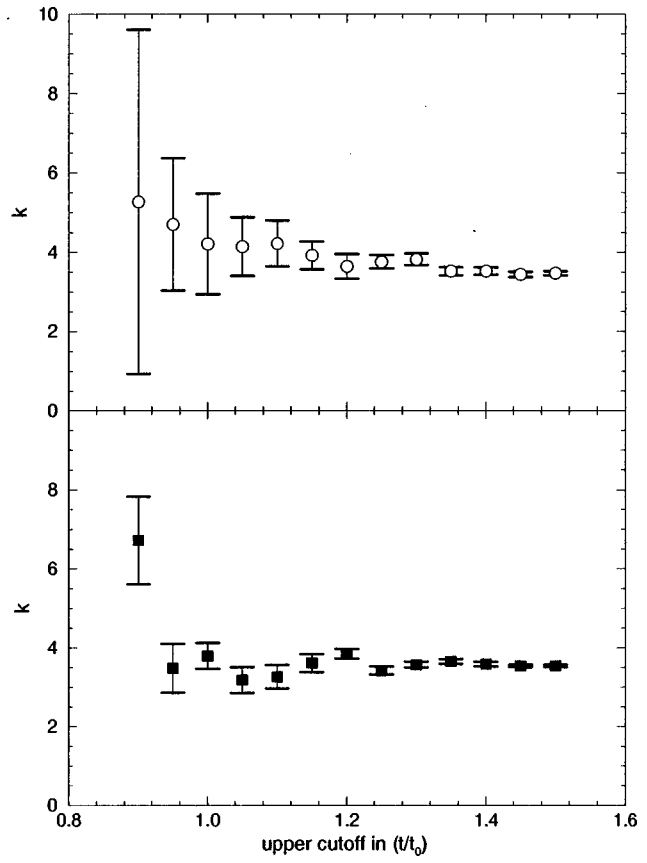

FIG. 8. Estimates for k, the number of intermediate assembly stages in the kinetic theory (16)–(19), based on fits of the form (35) to points in the experimental time series having t/t_0 less than an upper cutoff.

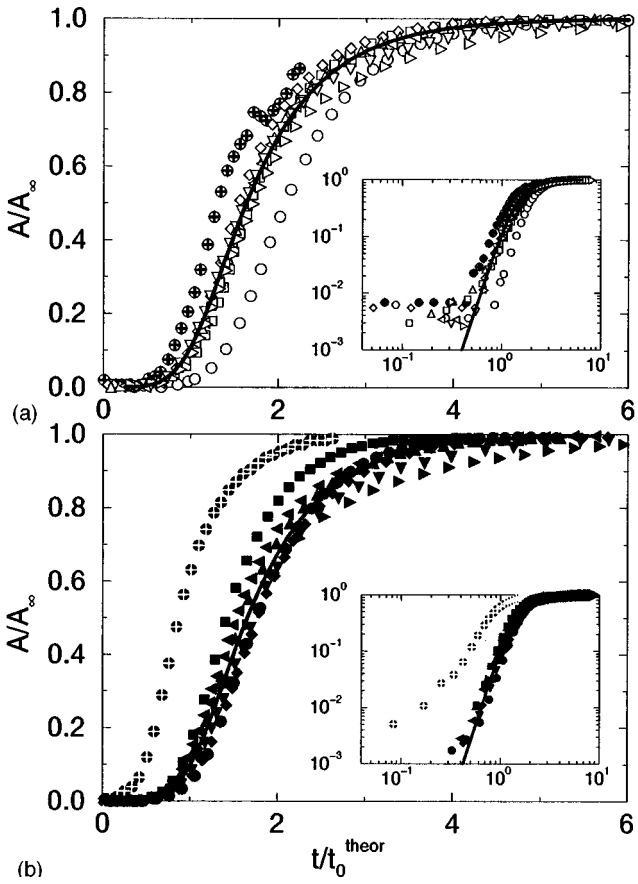

FIG. 9. Two-parameter fits of the theoretical turbidity to collapsed experimental time series. The data collapse shown here is not as good as that shown in Fig. 5 because time was rescaled in Fig. 5 with the t_0 values read off the time series, while here it is rescaled with t_0^{theor}. Also, the present figure shows all series, including obvious outliers. (a) Fitting to time series 3–8 in data set A, as ranked by final turbidity, gives the curve shown and parameter values given in the second line of Table I. The two outlier series, shown as circles with and without crosses, are series 1 and 2, and are not included in the fit. Table I also gives parameters resulting from a fit to series 3–6. (b) Fit to time series 2–8 in data set B, resulting in parameter values given in the fourth line of Table I. The outlier series, shown as filled circles with crosses, is series 1, and is not included in the fit. Table I also gives parameters resulting from a fit to series 2–7.

series, we face that k should have the same value for all time series, according to our scaling assumption. We therefore calculated the mean of the k values found for individual series and the variance on this mean, and estimated the common k value by the calculated mean, while estimating the quality of this estimate by the magnitude of the variance; see Fig. 8.

However, since the form (35) is true only for t values so small that terms of order t^{k+4} and higher can be neglected, as we have done, our fits of this form to all data up to a cutoff time will depend on the value of the cutoff time, except in the limit where this cutoff is taken to vanish. So at large cutoff times our estimate has systematic errors in it, but a fairly small error bar, since we fit to many data points. Conversely, as the cutoff time is reduced, the systematic errors are reduced, but the error bars on the estimate grow, because the k values that we average over show more scatter when obtained from fits to fewer data points; see Fig. 8. This figure shows very similar results for data sets A and B, thus confirming the experimental reproducibility of our results. These results do not point convincingly to an integer value, however. But since one must be chosen, $k=4$ is the best choice, and certainly in agreement with Fig. 8, though the value 3 that we found with a less refined method in [18] is not entirely excluded.

VIII. THE SIZE OF THE STABLE NUCLEUS

With both k and m known, we also know the number n, of tubulin hetero dimers it takes to form the stable nucleus, according to our model. The size of the nucleus is

$$n=n_0+n_1+\cdots+n_k=m(k+2), \tag{36}$$

so we conclude that the nucleus contains $n=18$ monomers. This number is close to the typical number of protofilaments, 14, in self-assembled microtubules [29]. It is also close to the number of hetero dimers it would take to form a lock-washer structure similar to that formed by tobacco mosaic virus' coating protein as a first step in its polymerization.

IX. RATE CONSTANTS

We fitted the theoretical turbidity $A(t)=A_\infty\,[1-c(t)/c_0]$ to the experimental time series, using the rate constants as fitting parameters, see Fig. 9. The theoretical turbidity was found by inserting Eqs. (25) and (28) with $m=3$ and $k=4$ in

TABLE I. Rate constants resulting from fits of model to experimental time series. The first four lines of table entries give results for two different fits of the theory to each of the collapsed data sets A and B, as illustrated in Fig. 9. The first line of entries resulted from a fit to time series number 3–6 in data set A, when the series are numbered according to ascending final turbidity. The second line of entries resulted from a fit to time series number 3–8 in data set A, the third line to series 2–7 in data set B, and the fourth line to series 2–8 in data set B. The following lines of entries in the table resulted from individual fits of the theory to individual time series, each of which is identified in column I by its final turbidity. Columns II and III: Values for parameters $\Pi_{i=0}^{k+1} f_i$ and $f_1 = f_2 = f_3 = f_4$ found by fitting model to given time series. Column IV: χ^2 per degree of freedom for the fit. Column V: The data set that the time series belongs to.

I	II	III	IV	V
A_∞ (cm^{-1})	$\Pi_{i=0}^{k+1} f_i$ (cm^{18}/min^6)	f_1 (cm^3/min)	χ^2_{PDF} (dimensionless)	Data set
	164	1.2	7.9	A, 3–6
	258	2.0	21	A, 3–8
	209	1.6	56	B, 2–7
	343	2.4	152	B, 2–8
0.142	499	3.5	0.5	B
0.146	372	2.7	0.4	A
0.236	74	-0.19	0.3	B
0.274	52	-0.76	0.1	A
0.279	84	0.14	0.8	B
0.338	84	0.11	0.3	A
0.365	134	0.82	0.5	A
0.371	115	0.64	1.9	B
0.456	168	1.3	1.4	A
0.471	236	1.9	5.6	B
0.542	208	1.6	4.8	B
0.582	205	1.6	3.1	A
0.672	328	2.4	78	B
0.703	421	2.8	23	A
0.768	582	3.3	6.1	A
0.772	1693	5.4	251	B

Eq. (15) and fitting its five parameters, f_1, f_2, f_3, f_4, and $\Pi_{i=0}^{5} f_i$, to the experimental data. For both data sets A and B and in several fits with different initial values and stopping criteria, we found $f_1 = f_2 = f_3 = f_4$ up to insignificant numerical differences. We consequently chose to *assume* this identity, and then fit again, now with a total of only two fitting parameters. Figure 9 shows the latter fits. The parameter values obtained from fits to data sets A and B do not differ significantly. They are given in the first four lines of Table I which show that the fitted parameter values are more sensitive to whether or not one includes the series for the fastest assembly processes in the fit, and less sensitive to whether the fit is to data set A or B.

The values given for $f_1 = f_2 = f_3 = f_4$ and $\Pi_{i=0}^{5} f_i$ in Table I are rather uncertain, but they are not physically unrealistic: The largest initial concentration, $c(0)$, used in the experiments gives rise to a final turbidity of 0.8 cm^{-1}. Consequently, at this initial concentration, one intermediate assembly product turns into the next one at a rate of $O(1)$ or less per minute, i.e., binding at most $O(10)$ monomers per minute. This rate should be compared with the rate at which microtubules bind monomers at the same concentration. Using 1 $cm^{-1} \approx 20$ μM tubulin as conversion factor between turbidity and tubulin mass ([17], Fig. 2), the estimate $f_5 \approx 1$ μm/min/μM (see Sec. IV A above), and that microtubules contain about 1700 monomers per micrometer, we have microtubules binding approximately 27 000 monomers per minute. Clearly, the creation of new microtubules is a much slower process than the growth of existing ones, even at this highest concentration studied here. Any other result would have been inconsistent with their existence. Because of the large uncertainty on the value found for $f_1 = f_2 = f_3 = f_4$, the value for $f_0 f_5$ that can be extracted from the value found for the product $\Pi_{i=0}^{5} f_i$ is too ill determined to be of interest.

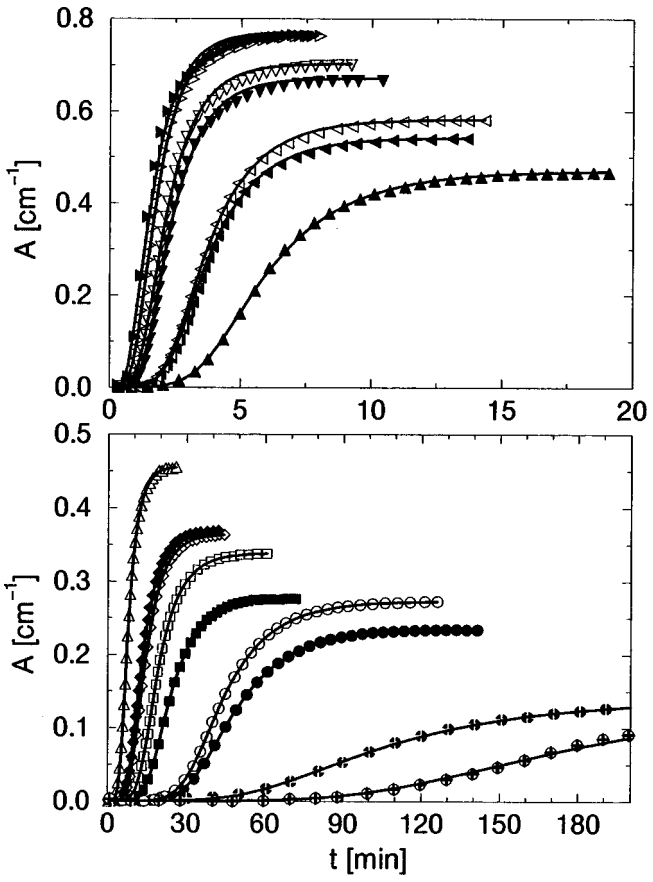

FIG. 10. Two-parameter fits of the theoretical turbidity to individual experimental time series. Parameter values resulting from fits are given in Table I.

In addition to the reasons already given for the fastest and slowest polymerizing time series, imperfections in the data collapse in Fig. 9 could be due to small changes in experimental conditions between the series, such as slight variations in temperature and buffer conditions. Such variations would give rise to different values for rate constants describing different time series, but presumably not change the kinetics itself. To allow for this situation, we fitted the theory to individual experimental time series, and found mostly very good individual fits; see Fig. 10 and Table I.

Figure 10 and column IV in Table I show that except for the very fastest nucleation processes in each data set, the

theory fits the experimental time series extremely well. It is not so surprising that the fastest processes are not modeled well. Already in Fig. 5, our phenomenological analysis showed that these fastest processes differ from the general data collapse. Since the model was developed to model the latter behavior, we cannot expect it to also accommodate the former. We could not exclude that it would either, however, so the fact that it cannot, when we specifically try to make it do it, indicates that the model is not arbitrarily flexible, but has characteristic properties that are felt even on the small scale of the scatter in the scaling collapse in Fig. 5. Section XII B discusses these properties of model vs experimental data.

Table I also shows that though the model fits the very slowest nucleation processes well, the fits can be absurd by yielding negative values for a positive definite rate constant. Again, we already knew from the phenomenological analysis that the slowest processes are anomalous relative to the scaling law in Eq. (7), hence should not be surprised that we get absurd results when we force the theory to fit time series that do not have the properties that guided us to the theory.

Figure 10 and Table I show that the theory fits very well the time series in the middle of the experimental window. Again, this is no surprise, since the theory was tailored to this purpose by tailoring it to the collapsed data which show the best collapse for these time series. The quality of these individual fits is, however, better than one could possibly have expected *a priori*. Figure 10 does not have sufficient resolution to show the quality of the best fits of the theory to the data. Figure 11 shows two-parameter fits of the theory to two experimental time series chosen from the middle of the experimental window.

When discussing the quality of these fits, we should mention that the χ^2 values given in column IV in Table I should not be taken too seriously. The error bars on the experimental time series' data points that these χ^2 values are based upon, are not true, independent statistical errors, but just the best we could come up with, namely, the instrument reading at vanishing input. The fact that we could fit several long time series with a χ^2 per degree of freedom which is significantly less than 1 is at least partly due to the fact that the theory was tailored to fit these data, i.e., we have not accounted correctly for the number of degrees of freedom when setting it equal to two, the number of independent rate constants fitted. But we may also have overestimated the errors on the data points, and/or they may be correlated.

More important, we note a clear trend with A_∞ in the values obtained for the fitted parameters, i.e., a systematic error relative to the assumed scaling behavior. This trend we noted already in the discrepancy to perfect collapse in Fig. 5. Since the theory was designed to be a scaling theory, it obviously cannot describe these scaling violations. So when we force it to model the individual time series, the scaling violations show up in the fitted parameter values, the only place where the theory can accommodate them. The range covered by these fitted parameter values is indicative of how well we really know the parameter values obtained with the fit shown in Fig. 9.

The general conclusion resulting from these individual fits is (i) that the model describes the data exceedingly well when it does it best, (ii) that there are small, but systematic, scaling violations in the data, and (iii) that the theory developed here does not model the slowest and fastest nucleation processes for which we have experimental data. Natural explanations of this last point were given above, and more are given below.

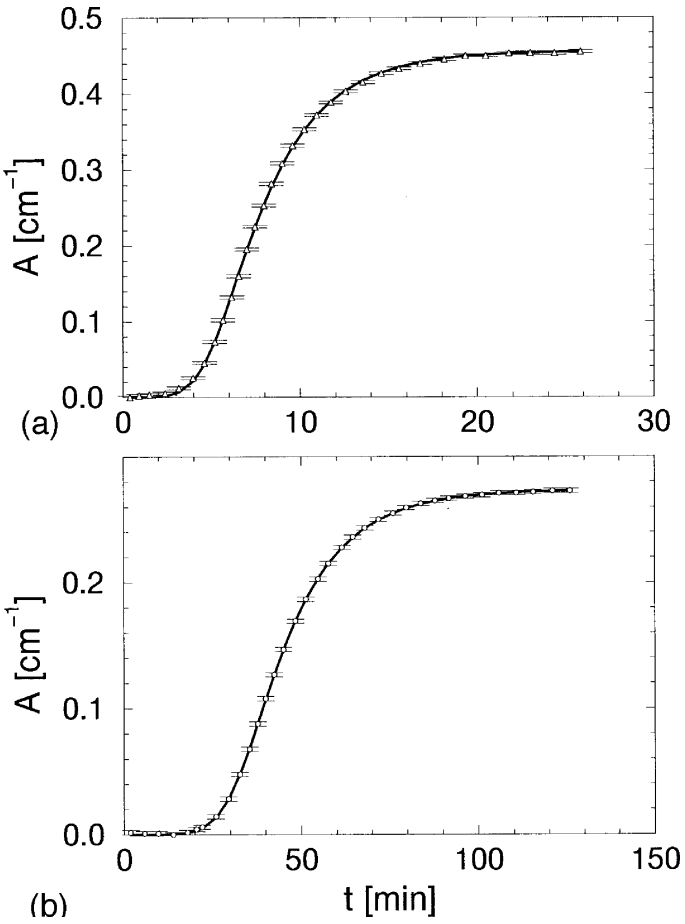

FIG. 11. Two of the best fits in Fig. 10, enlarged to make error bars and quality of fit visible. (a) Time series with $A_\infty = 0.456$ cm^{-1}. (b) Time series with $A_\infty = 0.274$ cm^{-1}. The error bars given for the experimental data points are estimates. As estimator we use the instrument output at times so early that there was no input in the form of turbidity caused by microtubules; see the inset in Fig. 5.

X. TIME COURSE OF PRODUCTION RATES

Now that the experimental time series for the amount of final polymer have yielded a model for the pathway of assembly, we may follow that pathway, and see how it is traversed, i.e., follow in time the rates of production for its various intermediate products. Figure 12's top frame shows the tubulin concentration as a function of time in a typical nucleation process chosen from the middle of the experimental window, the one in data set A with final turbidity $A_\infty = 0.456$ cm^{-1}. The following frames show the production rates for the various intermediate assembly products as a function of time, with the bottom frame showing the rate of production of the final product, the microtubule polymer. The values for f_0 and f_1 used to produce this figure were those in Table I, i.e., this figure shows the time course of the production rates leading to the theoretical turbidity shown in Fig. 11(a).

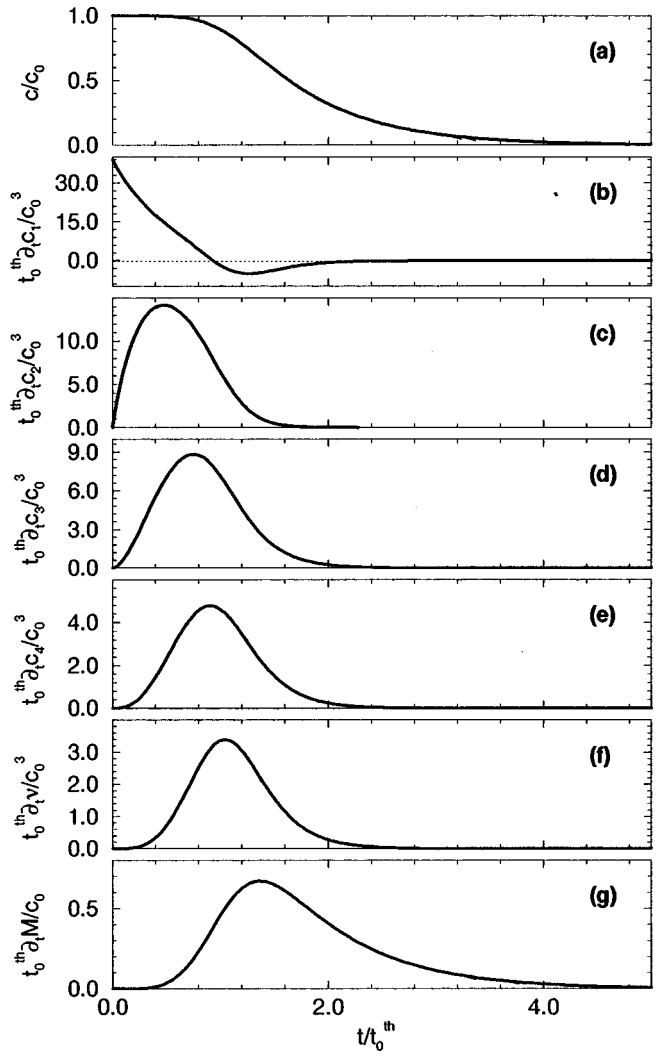

FIG. 12. Time dependence of tubulin concentration and production rates (in scaling units) for $f_0=168.48$ cm^{18}/min^6 and $f_1=1.347$ cm^3/min, as found from fit to experimental time series with $A_\infty=0.4560$ cm^{-1}. (a) Tubulin concentration c vs time t; in units of c_0 and $t_0^{\rm theor}$, respectively. (b)–(e) Rate of production $\dot{c}_i$ of intermediate assembly product i, $i=1,\ldots,4$, vs time; in units of $c_0^3/t_0^{\rm theor}$. (f) Rate of production $\dot{\nu}$ of stable nuclei vs time; in units of $c_0^3/t_0^{\rm theor}$. (g) Rate of production $\dot{M}$ of polymer vs time; in units of $c_0/t_0^{\rm theor}$.

Figure 12 illustrates, among other things, that the ith intermediate product is produced at a rate proportional to t^{i-1} at early times, which, combined with the vanishing initial values, gives that the ith intermediate product is present in amounts proportional to t^i initially, as discussed above. This i dependence of the early rates is just a manifestation of the model's property that the ith intermediate product is produced from the $(i-1)$th product. The relative locations of the maxima in the rates shown is another manifestation of this property. The vanishing of the rates at late times, on the other hand, is similar for all rates except the last, $\dot{M}$. The other five rates vanish as c^3, we know, and that includes $\dot{c}_1$, though it vanishes from negative values, because its production from monomers vanishes faster, as c^6, than the rate at which this first assembly product turns into the next one.

Figure 12(a) also shows that the tubulin concentration c remains almost constant initially: $c/c_0\approx 1$ up to the tenth time, $t_0^{\rm theor}$. This is understood by noting that M, the amount of final and *sixth* product, grows as t^6 initially, and therefore $c/c_0=1-M/M(\infty)=1-O(t^6)$ according to Eq. (15). This slow initial decrease of the tubulin concentration was established as a mathematical property valid at infinitesimal times t in Sec. VII A above, and used to determine the number of equations in the kinetic model. Figure 12(a) now shows that it is a good approximation up to the tenth time, a strong indication that our procedure was at least *self-consistently* correct.

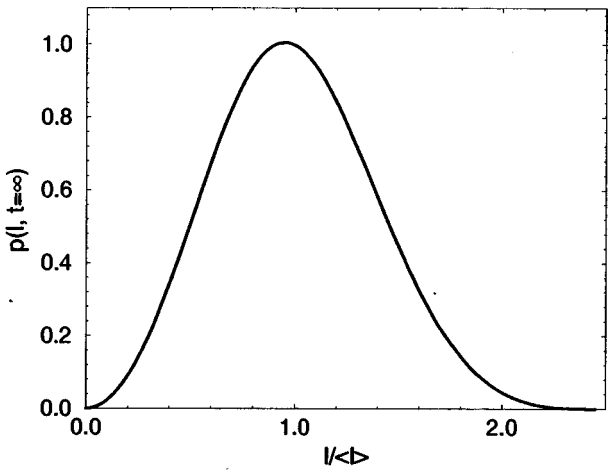

FIG. 13. Length distribution of microtubules at the end, $t=\infty$, of the nucleation-polymerization process described also in Fig. 12. The zeroth and first moment of the distribution were normalized to unity, because the turbidity measurements analyzed here cannot yield absolute numbers, either for lengths or for numbers of microtubules. The distribution's form at small and large values of ℓ is given in Eqs. (44) and (46), respectively, with $m=3$ and $k=4$.

The scenario invoked in Sec. II C to explain the turbidity's exponential approach to its asymptotic value is also illustrated by Fig. 12: The rate at which new microtubules is formed, $\dot{\nu}$, clearly vanishes before the tubulin concentration does. So at the latest times there is an essentially fixed number of microtubules present. They grow from the remaining tubulin, at a rate simply proportional to the remaining amount of tubulin; compare the latest part of the curves in the top and bottom frames in Fig. 12.

XI. THE DISTRIBUTION OF MICROTUBULE LENGTHS

A. Theoretical results

Figure 13 shows the theoretical final length distribution, $p(\ell;t=\infty)$, of the microtubules formed in the nucleation-polymerization process described also in Fig. 12. Since we can determine neither lengths nor numbers of microtubules from turbidity time series, the distribution shown is the relative one, normalized to unity,

$$\int_0^\infty d\ell\, p(\ell;\infty)=1, \tag{37}$$

and the length it depends on is also relative,

$$\int_0^\infty d\ell\, \ell\, p(\ell;\infty)=1. \tag{38}$$

We found this length distribution by combining our knowledge of the rate $\dot{\nu}(t)$ at which microtubules form at any time t with our knowledge of the velocity $f_{k+1}\times c(t)$ with which they grow. Thus a microtubule having length ℓ at time $t=\infty$ was created at a time t related to ℓ by

$$\ell = f_{k+1}\int_t^\infty dt'\, c(t'). \tag{39}$$

At that time of creation, t, microtubules were created at the rate $\dot{\nu}(t)$. Thus the number of microtubules at time infinity with lengths in an interval $d\ell$ at ℓ is

$$p(\ell,\infty)d\ell = \dot{\nu}(t)dt, \tag{40}$$

where dt is related to $d\ell$ through

$$d\ell/dt = f_{k+1}c(t), \tag{41}$$

so that

$$p(\ell,\infty)=\frac{\dot{\nu}(t)}{f_{k+1}c(t)}=\frac{f_k}{f_{k+1}}c_k(t)c(t)^{m-1}. \tag{42}$$

This is the distribution shown in Fig. 13. Similar arguments give $p(\ell;t)$ at any finite time t. These distributions at earlier times are, however, just the distribution shown in Fig. 13 translated towards shorter ℓ values and truncated at $\ell=0$.

Our analytical understanding of early and late nucleation and polymerization, as described by our model, translates into a similar understanding of the length distribution for the longest and shortest microtubules. The shortest microtubules were formed at the latest times, where $c_k(t)=c_k(\infty)$, while $c(t)$ vanishes as a simple exponential. Used in Eq. (39), this gives

$$\ell \propto c(t) \quad \text{for } \ell \approx 0, \tag{43}$$

where t is the time of creation of the microtubule of length ℓ. Consequently, by Eq. (42),

$$p(\ell;\infty)\propto \ell^{m-1} \quad \text{for } \ell\approx 0. \tag{44}$$

The maximal length a microtubule can have, according to our nucleation model, is

$$\ell_{\max} = f_{k+1}\int_0^\infty dt'\, c(t'). \tag{45}$$

The longest microtubules were formed at the earliest times, where $c(t)=c_0$, hence $\ell_{\max}-\ell \propto t$, and $c_k(t)\propto t^k$. Consequently,

$$p(\ell;\infty)\propto(\ell_{\max}-\ell)^k \quad \text{for } \ell\approx\ell_{\max}. \tag{46}$$

B. Experimental triple test

The length distribution of microtubules is experimentally measurable. It has been measured in other experiments by fluorescence microscopy [30], by electron micrography [31,32], and its Fourier transform by synchroton radiation ([33] and references therein). The formulas just derived show that an experimental measurement of the final length distribution of microtubules, obtained after nucleation and polymerization has run its course, can provide a *triple* test of the theory presented here. The simplest test consists in measuring the length distribution experimentally and comparing it with Fig. 13. But with sufficient experimental data, there are two additional tests of the theory: Its two integer parameters, m and k, are found not only from the turbidity time series, but again in the final length distribution. While this second determination of k related directly to that obtained from the time series, the second determination of m relates to a particular stage in the nucleation process, the formation of microtubules from the last intermediate assembly product, as seen from Eq. (42). This stage cannot be observed as directly in the turbidity time series as it can in this analysis of the final length distribution.

XII. BEYOND SCALING

Although the theory presented above describes the turbidity time series with precision, it is only an approximate theory. It was obtained by assuming scaling, a property that is only approximately satisfied by the experimental data. But because it is satisfied to a good approximation, the theory presented above is also a good starting point for a search for a more precise theory.

A. Systematic scaling violations, I

Clues to the properties of an improved theory must be found in the systematic differences between the experimental data and the scaling theory derived above. To this end, we observe that the experimental time series analyzed here actually contain more information than we have used. This shows up in two ways. First, the scaling violations that one can observe in Fig. 5 at late assembly times, display a trend with A_∞: the larger the initial tubulin concentration is, the slower is the approach of the time series to its asymptotic value, when measured in scaling variables, as done in that figure. Second, the approach to the asymptote is exponential in time, as illustrated phenomenologically in Fig. 3, and following theoretically from Eq. (6). But while we found the tenth time, t_0, proportional to A_∞^{-3}, the characteristic times, t_∞, of this exponential approach, defined as

$$A_\infty - A(t) \propto \exp(-t/t_\infty) \tag{47}$$

do not quite obey this power law; see Fig. 14.

If the experimental time series did scale perfectly and with $t_0\propto A_\infty^{-3}$, then $t_\infty/t_0^{\text{theor}}$ would be constant, independent of A_∞, in Fig. 14. The plot shows a trend, however, or the two largest turbidities in each data set, A and B, label outliers. These outliers are not statistical in nature, but systematic, since both data sets A and B display them for both series with largest final turbidities.

Note, however, that by focusing on $A_\infty - A(t)$ at late times we are focusing on only a small part of the whole value of $A(t)$. So there is no grave contradiction in practice: $A(t)$ itself can scale with $t_0\propto A_\infty^{-3}$ to a good approximation,

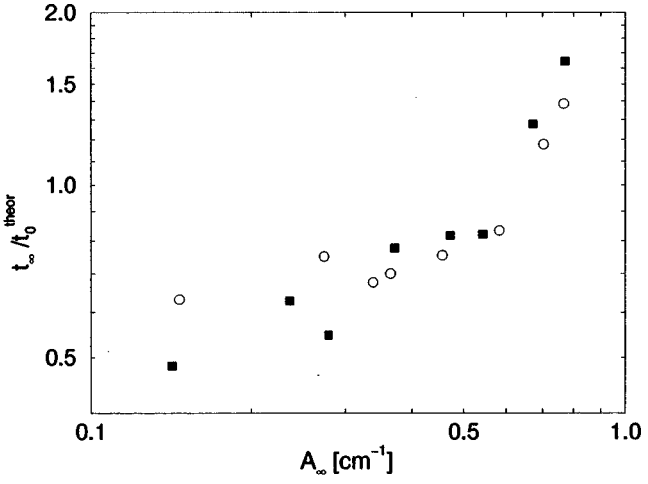

FIG. 14. Characteristic time t_∞ of each experimental time series' exponential approach to its asymptotic turbidity A_∞ in units of its theoretical tenth time $t_0^{\text{theor}}=(0.41\pm0.01)$ min/cm$^3\times A_\infty^{-3}$—plotted against its asymptotic turbidity, A_∞.

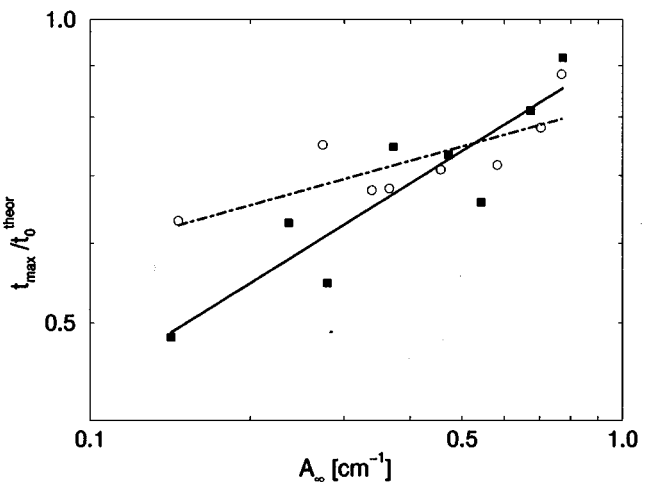

FIG. 15. Characteristic time of maximal relative polymerization rate, $t_{\max}=1/\max_t[-d\log_{10}c(t)/dt]$ in units of $t_0^{\text{theor}}=(0.41\pm0.01)$ min cm$^3\times A_\infty^{-3}$ plotted for each experimental time series against its asymptotic turbidity A_∞. The straight lines through the data are separate fits to data sets A and B, and have slopes 0.15 ± 0.05 and 0.33 ± 0.06, respectively. In the case of perfect scaling these slopes should not differ significantly from zero.

while the small, late increments in $A(t)$ simultaneously show significant scaling violations.

B. Features in data that ordinary differential equations cannot model

Focusing on $A_\infty - A(t)$ at late times, reveals a *qualitative* limitation, as well, of the theory presented here. Plotted as in Fig. 3, the *slope* of the time series is

$$\frac{d}{dt}\log_{10}[A_\infty - A(t)] = \frac{d}{dt}\log_{10}c(t) = -\frac{c_0}{M(\infty)} f_{k+1}\nu(t) \tag{48}$$

according to Eqs. (15) and (19), i.e., the slope equals the number of microtubules that have been nucleated, $\nu(t)$, up to a constant. According to our theory's Eq. (18), this number is nondecreasing, *microtubules never disappear*. This is a technically important feature of the theory, because it makes it possible to formulate the kinetic equations for the total amount of polymer formed as a finite number of ordinary differential equations: The amount of polymer grows by addition of monomers to existing microtubules (including stable nuclei), and the number of these microtubules and nuclei is entirely given by the kinetics describing their formation in a finite number of steps, as described above.

If, on the other hand, the number of microtubules *decreases* at any point in time—as we observe in the rightmost time series in Fig. 3 whose steepest slopes are steeper than their final slopes—then, obviously, we observe a phenomenon that is beyond our theory. No theory based on a finite number of ordinary differential equations can describe this phenomenon correctly. Since microtubules disappear by depolymerization from their ends, only a theory having the *length distributions* of growing and shrinking microtubules as dynamical variables, can describe this correctly. Such a theory involves partial differential equations, as in the model for microtubule oscillations described in [21].

C. Systematic scaling violations, II

The time series corresponding to the largest initial tubulin concentrations signal some disappearance of microtubules at intermediate times when analyzed in terms of our theory, we just saw, hence cannot be fully reproduced by our theory. The insights of the preceding section may explain the outliers at the largest A_∞ values in Fig. 14. The too large values for $t_\infty/t_0^{\text{theor}}$ correspond to too small values for the final number of microtubules because

$$t_\infty^{-1} = -\lim_{t\to\infty}\frac{d}{dt}\log_{10}[A_\infty - A(t)] \propto \nu_\infty . \tag{49}$$

So instead of the final number of microtubules present we focus on their *maximal* number, and the characteristic time $t_{\max}$ for the corresponding polymerization rate [34],

$$t_{\max}^{-1} = \max_t\left(-\frac{d}{dt}\log_{10}[A_\infty - A(t)]\right). \tag{50}$$

For time series showing no disappearance of microtubules, $t_{\max}=t_\infty$, and this is the case for most series. But where there is a difference, our theory has a better chance of describing the dynamics only up to the time where the number of microtubules is maximal.

Figure 15 shows $t_{\max}/t_0^{\text{theor}}$ plotted against A_∞. Comparing with Fig. 14, we note that the outliers have disappeared. (Note change of scale on second axis.) But there is still a significant trend in the plot, i.e., significant scaling violations.

The fact that we can isolate a systematic scaling violation in the time series shows that the scaling theory presented here does not exhaust the experimental information hidden in the series.

We have tried to modify and extend the theory in such ways that the scaling violations described here are accommo-

dated in a natural, perturbative way. A natural starting point for minimal modifications of the theory is the theory's cooperative kinetics. We have tried to time resolve more steps of the assembly pathway already established with the scaling theory. We have varied the cooperative nature of steps by floating n_i in combined fits of the theory to whole data sets, A and B, in a manner that affects the theory mainly at late times, where scaling violations show in the data, while barely affecting the theory at early times, where the data scale well. We have tried to form the first intermediate assembly product in two parallel pathways, one being the one-step procedure described above, the other being a two-step procedure combining three monomers at a time. In this way we did find theories with modest scaling violations which fitted the experimental time series better than our scaling theory. But the approach was entirely *ad hoc*, the improvement was guaranteed by the fact that we added new fitting degrees of freedom to an already good theory, and finally the improvement was not dramatic, hence giving no clue to a less *ad hoc* approach. Add to this that the scaling violations we try to describe occur at late times, where they are mixed up with the effect of disappearing microtubules, a phenomenon beyond any small modification of the theory. Then we have given our reasons for not pursuing the scaling violations further.

XIII. DISCUSSION

A. Scaling violations

We have not overlooked the fact that we introduced an approximation with Eq. (13). However, one should *not* try to ''improve'' the theory by replacing Eq. (13) with Eq. (14). For one thing, this would introduce an additional unknown parameter, c_0, by severing its simple proportionality with A_∞. But from the experimental fact that typical microtubules contain thousands of monomers it also follows that the approximation introduced with Eq. (13) is *very* good, much too good for the difference to Eq. (14) to explain the scaling violations in the data.

B. Relationship between turbidity and polymer mass

We have assumed a simple proportionality between the total amount of polymerized mass and the measured turbidity, and this assumption played a key role in our arguments, because it allowed us to identify the relative turbidity, i.e., A/A_∞, with the relative amount of polymer formed, and further, by virtue of Eq. (13), with the relative concentration of tubulin. The assumed proportionality allowed us to rid ourselves of the unknown absolute scales of polymer mass and tubulin concentration by working with relative amounts, and it also allowed us to use directly the relative turbidity for the relative polymer mass, instead of corrupting the good precision of turbidity measurements with the bad precision of biochemical assays in a calibration of the turbidity's relationship to polymer mass.

The assumption of proportionality is only correct, however, in a reasonable approximation for microtubules with lengths exceeding the wavelength of the light used to measure the turbidity, here 350 nm ([25], Fig. A2) as discussed above. Gaskin, Cantor, and Shelanski have demonstrated experimentally that there is, indeed, within a few percent, a simple proportionality between polymerized mass and measured turbidity for turbidities from 0.1 to 0.4 caused by microtubules nucleated and polymerized in bulk, after equilibrium has been acquired ([35], Fig. 4). Related results were obtained by Voter and Erickson ([17], Fig. 2). However, Gaskin, Cantor, and Shelanski also demonstrated that the turbidity to some extent depends on the length distribution of the microtubules: By 30 seconds of sonication they reduced the average length of a sample of microtubules by a factor 5 or more, judging from micrographs. The turbidity at 350 nm consequently dropped by approximately 15%. But sonication for more than 2 minutes actually *increased* the turbidity above that of control samples, so it is not entirely clear what went on, especially whether the total amount of polymer remained constant during and after sonication. Thus it might be of some interest to repeat this experiment with microtubules stabilized, e.g., with glycerol and no free tubulin present in order to test to which extent the turbidity depends only on the summed total length of polymer, and not on the length distribution of the polymers.

C. Microscopic interpretation of the kinetic model

As it stands, the theory fitted to the data gives $f_1=f_2=f_3=f_4$. This identity combined with the identity $n_1=n_2=n_3=n_4=m$ indicates that it is the *same* mechanism that stabilizes each of the intermediate assembly aggregates. A single allosteric effect involving $m=3$ tubulin heterodimers could be a simple microscopic explanation of this identity. In this microscopic picture, triplets of tubulin hetero dimers are added successively to the sixplet first formed, to form the nucleus of 18 dimers. One should be very cautious, however, about such a microscopic interpretation, because there is a simple, mathematical interpretation of the identity $f_1=f_2=f_3=f_4$: We saw above from the exact solution to the model that any fit to the experimental data which would result in nonequal values for $f_1, \ldots, f_4$, would also be obtained from any permutation of these parameters. Thus the χ^2 landscape over the space of fitting parameters has as many degenerate minima as there are different permutations of the four fitting parameters $f_1, \ldots, f_4$. The simplest landscape is one with only one minimum, corresponding to $f_1=f_2=f_3=f_4$. Thus relatively rich and complex experimental data are necessary to sustain what appears to be a generic set of values for $f_1, \ldots, f_4$, while the simplest possible situation, data sustaining only a single minimum in χ^2, leads to identical parameter values $f_1, \ldots, f_4$, hence an identity in the model's reactions which seems to require a special mechanism to assure its presence. There is, of course, also a special mechanism in effect that assures the identity: It is *symmetry* under the permutation group of four elements, S_4, that, in the language of high-energy physics, ''protects'' the identity of the rates.

D. Support for model from other experiments

The model presented here is somewhat supported by independent experiments done at 15 °C–30 °C, which measured the nucleation rate $d\nu/dt$ at constant tubulin concentration by counting the number of individual microtubules being created, as seen through a microscope [36]. This rate

was found proportional to the tubulin concentration to the power 12 ± 2, which does not seriously disagree with the power 18 predicted here, considering the errors possible in both approaches. Rather, one should focus on the fact that both approaches give values in the same low range.

But if we tentatively do take seriously the value we have found for the size of the stable nucleus, we note that its 18 hetero dimers are very close in number to the typical number of protofilaments in microtubules, 13, 14. This then suggests that the stable nucleus may be a single ring or protohelix (''lock-washer'') like those formed by the coating protein of tobacco mosaic virus [37,3]. Remarkably, γ-tubulin forms ringlike structures of size similar to our nucleus in centrosomes, where it participates in *in vivo* nucleation of microtubules, though it is not known exactly how [38]. It has, however, been demonstrated *in vitro* that γ-tubulin binds tightly and exclusively to the minus ends of microtubules in a saturable fashion with a stoichiometry of 12.6 ± 4.9 molecules per microtubule [39]. Taken together, these experimental results indicate that a ring of γ-tubulin the size of our nucleus nucleates microtubules in centrosomes. Hence it is natural to speculate whether the nucleus discussed in the present paper has the same shape.

E. The value of phenomenological data analysis and systematic modeling

Even if the reaction pathway found here turns out to be no more than a mathematical mirage, it remains the most precise mathematical substrate of the information in the data, until a better fitting model is developed. Our systematic derivation of the model should also be of value by itself, i.e., as a procedure. Compare it, e.g., with the way that the relevant Oosawa model was found in [9]: There, two time series for the self-assembly of actin were analyzed separately, and Oosawa's model was found to fit both well, but with ill determined parameters in both cases. Only after some roundabout was it concluded that only one set of parameters would fit both experimental time series *simultaneously*. The Oosawa model with zero off rate that was the final result of that analysis, is scale invariant. So are the experimental time series that it fits, we may conclude. But that property could then have been established *phenomenologically* from the start, in a model-independent manner, and *then* the parameters of Oosawa's model could have been determined unambiguously in a straightforward *single* fit of its scaling form to the collapsed data.

XIV. CONCLUSIONS

Before one can conclude anything regarding a scenario for the molecular pathway of microtubule self-assembly, the kinetic model derived here must be supplemented with more and independent evidence. It would also be interesting to measure turbidity time series at different temperatures. The slower kinetics and longer tubulin lifetimes at lower temperatures make it possible to study assembly at concentrations inaccessible at $37\,^{o}$C. Similarly, it would be interesting to monitor self-assembly from tubulin liganded with the nonhydrolyzable GTP analog GMPCCP [guanylyl-(α,β)-methylene-diphosphonate], since such tubulin nucleates faster [23], hence allows us to study self-assembly at lower concentrations. If the scaling behavior described here is observed at different temperatures and concentrations as well, that provides further evidence that there is, indeed, a definite assembly mechanism responsible for the data.

For now, we may conclude about turbidity measurements that this simple physical method can yield data of sufficient quality to sustain a rather rigorous mathematical analysis. About the mathematical analysis, we may conclude that it sometimes is possible to solve the *inverse problem*, to find a reaction's path from its products. Thus, by combining a simple, but precise, physical measure with a systematic mathematical analysis we have created a ''microscope'' through which one apparently may ''observe'' some otherwise inaccessible details of a biochemical self-assembly process. It would be interesting to obtain independent confirmation of these ''observations'' and to study other processes in this manner.

ACKNOWLEDGMENTS

We are grateful to W. A. Voter and H. P. Erickson for sending us their turbidity data and discussing them with us. H.F. thanks S. Leibler for hospitality and discussions. H.F. was partially supported by The Danish Natural Science Research Council, Grant No. 11-0244-1, and by Julie Damm's Studiefond.

[1] L. D. Landau and E. M. Lifshitz, *Mechanics*, Course of Theoretical Physics Vol. 1, 3rd ed. (Pergamon Press, New York, 1976), p. 52.
[2] F. J. Dyson, in *Studies in Mathematical Physics*, edited by E. H. Lieb, B. Simon, and A. S. Wightman (Princeton University Press, Princeton, NJ 1976).
[3] D. Voet and J. G. Voet, *Biochemistry* (John Wiley & Sons, Inc., New York, 1990), Chap. 13, pp. 339 and 340.
[4] A. G. Loewy, P. Siekevitz, J. R. Menninger, and J. A. N. Gallant, *Cell Structure and Function*, 3rd ed. (Saunders College Publishing, Philadelphia, 1991).
[5] F. Oosawa and M. Kasai, J. Mol. Biol. **4**, 10 (1962).
[6] F. Oosawa and S. Higashi, Prog. Theor. Biol. **1**, 79 (1967).
[7] F. Oosawa and S. Asakura, *Thermodynamics of the Polymerization of Protein* (Academic Press, New York, 1975), pp. 41–55.
[8] A. Wegner and J. Engel, Biophys. Chem. **3**, 215 (1975).
[9] A. Wegner, J. Mol. Biol. **108**, 139 (1976).
[10] A. Wegner and P. Savko, Biochemistry **21**, 1909 (1982).
[11] L. S. Tobacman and E. D. Korn, J. Biol. Chem. **258**, 3207 (1983).
[12] J. Hofrichter, P. D. Ross, and W. A. Eaton, Proc. Natl. Acad. Sci. USA **71**, 4864 (1974).
[13] F. A. Ferrone, J. Hofrichter, H. R. Sunshine, and W. A. Eaton, Biophys. J. **32**, 361 (1980).
[14] F. A. Ferrone, J. Hofrichter, and W. A. Eaton, J. Mol. Biol. **183**, 611 (1985).
[15] P. E. Prevelige, D. Thomas, and J. King, Biophys. J. **64**, 824 (1993).

[16] H. Flyvbjerg, T. E. Holy, and S. Leibler, Phys. Rev. E **54**, 5538 (1996).
[17] W. A. Voter and H. P. Erickson, J. Biol. Chem. **259**, 10 430 (1984).
[18] H. Flyvbjerg, E. Jobs, and S. Leibler, Proc. Natl. Acad. Sci. USA **93**, 5975 (1996).
[19] T. Mitchison and M. Kirschner, Nature (London) **312**, 232 (1984).
[20] T. Mitchison and M. Kirschner, Nature (London) **312**, 237 (1984).
[21] E. Jobs, D. E. Wolf, and H. Flyvbjerg, Phys. Rev. Lett. **79**, 519 (1997).
[22] H. P. Erickson and D. Pantaloni, Biophys. J. **34**, 293 (1981).
[23] A. A. Hyman *et al.*, Mol. Biol. Cell **3**, 1155 (1992).
[24] D. N. Drechsel, A. A. Hyman, M. H. Cobb, and M. W. Kirschner, Mol. Biol. Cell **3**, 1141 (1992).
[25] B. J. Berne, J. Mol. Biol. **89**, 737 (1974).
[26] D. K. Fygenson, E. Braun, and A. Libchaber, Phys. Rev. E **50**, 1579 (1994).
[27] R. F. Gildersleeve *et al.*, J. Biol. Chem. **267**, 7995 (1992).
[28] J. R. Simon, S. F. Parsons, and E. D. Salmon, Cell Motil. Cytoskel. **21**, 1 (1992).
[29] D. Chrétien *et al.*, J. Cell Biol. **117**, 1031 (1992).
[30] D. Kristofferson, T. Mitchison, and M. Kirschner, J. Cell. Biol. **102**, 1007 (1986).
[31] S. R. Martin *et al.*, Biochim. Biophys. Acta **914**, 96 (1987).
[32] P. M. Bayley, M. J. Schilstra, and S. R. Martin, J. Cell. Sci. **93**, 241 (1989).
[33] A. Marx *et al.*, in *Synchrotron Radiation in the Biosciences*, edited by B. Chance *et al.* (Clarendon Press, Oxford, 1994), Chap. 2.4, pp. 158–168.
[34] The notation may confuse, so we emphasize: $t_{\max}$ itself is *not* a maximized time. On the contrary. It is the characteristic time of a process at its maximal rate, so $t_{\max}$ itself is a minimum among characteristic times. Obviously, it is also not the time when the maximum occurs.
[35] F. Gaskin, C. R. Cantor, and M. L. Shelanski, J. Mol. Biol. **89**, 737 (1974).
[36] D. K. Fygenson *et al.*, Phys. Rev. E **51**, 5058 (1995).
[37] A. C. H. Durham, J. T. Finch, and A. Klug, Nature (London) **229**, 38 (1971).
[38] M. Moritz *et al.*, J. Cell Biol. **130**, 1149 (1995).
[39] Q. Li and H. C. Joshi, J. Cell Biol. **131**, 207 (1995).